Large-Scale Vertical Velocity, Diabatic Heating and Drying Profiles Associated with Seasonal and Diurnal Variations of Convective Systems Observed in the GoAmazon2014/5 Experiment

Shuaiqi Tang[1], Shaocheng Xie[1], Yunyan Zhang[1], Minghua Zhang[2], Courtney Schumacher[3], Hannah Upton[3], Michael P. Jensen[4], Karen L. Johnson[4], Meng Wang[4], Maike Ahlgrimm[5], Zhe Feng[6], Patrick Minnis[7] and Mandana Thieman[8]

[1]Lawrence Livermore National Laboratory, Livermore, CA, 94550, USA
[2]School of Marine and Atmospheric Sciences, tony Brook University, Stony Brook, NY, 11794, USA
[3]Department of Atmospheric Sciences, Texas A&M University, College Station, TX, 77843, USA
[4]Brookhaven National Laboratory, Upton, NY, 11973, USA
[5]European Centre for Medium-Range Weather Forecasts, Shinfield Park, Reading RG2 9AX, United Kingdom
[6]Pacific Northwest National Laboratory, Richland,Washington, 99354, USA
[7]NASA Langley Research Center, Hampton, VA, 23681, USA
[8]Science Systems and Applications, Inc, Hampton, VA 23666, USA

Correspondence to: Shuaiqi Tang (tang32@llnl.gov)

Abstract. This study describes the characteristics of large-scale vertical velocity, apparent heating source (Q_1) and apparent moisture sink (Q_2) profiles associated with seasonal and diurnal variations of convective systems observed during the two intensive operational periods (IOPs) that was conducted from 15 February to 26 March 2014 (wet season) and from 1 September to 10 October 2014 (dry season) near Manaus, Brazil, during the Green Ocean Amazon (GoAmazon2014/5) experiment. The derived large-scale fields have large diurnal variations according to convective activity in the GoAmazon region and the morning profiles show distinct differences between the dry and wet seasons. In the wet season, propagating convective systems originating far from the GoAmazon region are often seen in the early morning, while in the dry season, they are rarely observed. Afternoon convective systems due to solar heating are frequently seen in both seasons. Accordingly, in the morning, there is strong upward motion and associated heating and drying throughout the entire troposphere in the wet season, which is limited to lower levels in the dry season. In the afternoon, both seasons exhibit weak heating and

strong moistening in the boundary layer related to the vertical convergence of eddy fluxes. A set of case studies of three typical types of convective systems occurring in Amazonia - i.e., locally-occurring systems, coastal-occurring systems and basin-occurring systems - is also conducted to investigate the variability of the large-scale environment with different types of convective systems.

1. Introduction

Amazonia is one of the major tropical convective regions in the global climate system. It provides moisture to the global hydrological cycle and energy to drive the global atmospheric circulation. Understanding convective systems over the Amazon region through observations is important for understanding and simulating global circulation and climate. However, most of Amazonia is covered by tropical forest with only a few observational sites. In order to collect the observations needed to improve our understanding of convective systems over Amazonia, several major field campaigns have been conducted in this area such as the Amazon Boundary Layer Experiments (Harriss et al., 1988; Harriss et al., 1990), the Large-Scale Biosphere-Atmosphere Experiment in Amazonia (LBA) (Silva Dias et al., 2002b), and the CHUVA project (Machado et al., 2014).

Recently, an internationally collaborative experiment, the Observations and Modeling of the Green Ocean Amazon (GoAmazon2014/5) (Martin et al., 2016), was conducted in the region around Manaus, Brazil from January 2014 to December 2015 with a focus on the aerosol and cloud life cycles and aerosol-cloud-precipitation interactions over tropical rainforests. Two 40-day Intensive Operational Periods (IOPs) were conducted in 2014 to investigate the seasonal variations of clouds and aerosols, as well as their interactions. IOP1 took place from 15 February to 26 March 2014 during the wet season, and IOP2 took place from 1 September to 10 October 2014 during the dry season. The goal of this study is to document and understand the seasonal variability and diurnal cycle of large-scale vertical velocity, heat and moisture budgets associated with the convective systems observed during the two IOPs in the GoAmazon2014/5 experiment.

The Amazon region has a significant seasonal variation in precipitation amount. Rainfall is approximately 300 mm per month during the wet season while it is close to 100 mm per month during the dry season (Tanaka et al., 2014). Many studies have examined the seasonal variation of clouds and precipitation in Amazonia (e.g. Harriss et al., 1988; Harriss et al., 1990; Fu et al., 1999; Fu et al., 2001; Schumacher and Houze, 2003; Machado et al., 2004; Li et al., 2006; Nobre et al., 2009; Marengo et al., 2012; Filho et al., 2015). Compared to the large variation in clouds and rainfall, the seasonal variation in CAPE is small (Machado et al., 2004; Martin et al., 2016). Martin et al. (2016) suggests that small perturbations in the large-scale circulation can drive dramatic changes in hydrological fields in this region. Few studies, however, have studied the seasonal variation of the diabatic heating and drying structures associated with the convective systems in the Amazon region.

The diurnal cycle of the atmosphere is an important feature that is poorly simulated in climate models. Many efforts have been made to observe and to understand the diurnal cycle over the Amazon basin using surface observations (e.g. Harriss et al., 1990; Cutrim et al., 2000; Machado et al., 2004; Tanaka et al., 2014) or satellite data (e.g. Minnis and Harrison, 1984; Greco et al., 1990; Janowiak et al., 2005; Burleyson et al., 2016). The diurnal cycle over the Amazon basin is complex because it is affected by three types of convective systems: locally-occurring systems (LOS) generated locally in the form of small convective cells (area less than 1000 km^2) with short life time (on the order of 1 hour), coastal-occurring systems (COS) initialized at the northeast coast of Brazil by the sea-breeze and propagating inland as squall lines, and basin-occurring systems (BOS) initialized in the Amazon basin in the form of mesoscale convective systems (MCS) with areas larger than 1000 km^2 (Greco et al., 1990). These systems reach Manaus, near the center of the Amazon basin, at different times of the day, causing a broad

peak of precipitation from morning to early afternoon (e.g. Machado et al., 2004; Tanaka et al., 2014; Burleyson et al., 2016). Schumacher et al. (2007) examined the diurnal cycle of the large-scale heating budget in the southwest Amazon during LBA, but used only two profiles per day, which do not capture the rapidly changing environment. In addition, the diurnal cycle over the highly deforested southwest Amazon is not necessarily representative of the more pristine central Amazonian rainforest.

In this study we use data collected from the comprehensive GoAmazon2014/5 field campaign to examine the seasonal and diurnal variations of the large-scale vertical velocity and heat and moisture budgets associated with the convective systems that occur in central Amazonia. Section 2 provides details of the data and method used to derive the large-scale profiles for the GoAmazon2014/5 experiment. Section 3 describes the synoptic conditions for the two IOPs. Sections 4 and 5 show the seasonal variation and diurnal cycle of the large-scale fields, respectively. Section 6 further investigates three selected cases representing different types of convective systems in the wet season. The summary and discussion are given in Section 7.

2. Data and Method

Due to the lack of an appropriate sounding array to capture the divergence and advection fields in the analysis domain, the large-scale vertical velocity and budgets analyzed in this study were derived by using, as a first guess, the 0.5°×0.5° European Centre for Medium-Range Weather Forecasts (ECMWF) analysis data that are subsequently constrained with domain averaged surface and top of atmosphere (TOA) observations. The upper-level fields from ECMWF analysis data are adjusted to conserve the vertical integration of mass, moisture and dry

static energy through a constrained variational analysis technique described in Zhang and Lin (1997) and Zhang et al. (2001). As indicated in Xie et al. (2004), the use of the surface and TOA observations as constraints improves the quality of the large-scale vertical velocity and budgets in operational analysis data and makes the data suitable for budget analysis and cloud modeling studies. An important by-product of this study is the derived large-scale forcing data (ARM Climate Research Facility, 2001) supporting modeling studies, which are available to the community at the Atmospheric Radiation Measurement (ARM) program Archive (http://iop.archive.arm.gov/arm-iop/0eval-data/xie/scm-forcing/iop_at_mao/).

Figure 1 shows the location of the GoAmazon2014/5 experiment and the analysis domain (the red octagon, referred to as the GoAmazon domain) used in this study, which is about 110 km in radius. The observational research sites and major cities near the region are also shown on the map. The required surface and TOA fluxes as the constraints for the variational analysis are constructed as follows. The precipitation used in this study is derived from the System for the Protection of Amazonia (SIPAM) S-band (10 cm wavelength) radar operated at Ponta Pelada airport, the center of the GoAmazon domain. The SIPAM radar reflectivity constant altitude plan position indicator (CAPPI) at 2.5 km above ground was used to generate the rain rate products using a single Z-R relation of $Z = 174.8R^{1.56}$ derived from Joss-Waldvogel disdrometer data obtained by the CHUVA campaign near Manacapuru during the wet season of early 2014. Other surface constraint variables, such as surface radiative fluxes and latent and sensible heat fluxes, are obtained from the broadband radiometer (ARM Climate Research Facility, 1994) and eddy correlation flux measurement system (ARM Climate Research Facility, 2003) at the ARM Mobile Facility site near Manacapuru (3.213°S, 60.598°W; "ARM site" in Figure 1). Observations of latent and sensible heat fluxes at two other Brazilian research sites - K34 ("ZF2"

125 in Figure 1) and the Amazon Tall Tower Observatory ("ATTO" in Figure 1) - are also used. The
126 TOA measurements of broadband radiative fluxes are estimated from the Thirteenth
127 Geostationary Operational Environmental Satellite (GOES-13) 4-km visible (0.65 μm) and
128 infrared window (10.8 μm) radiances using the narrowband-to-broadband (NB-BB) conversion
129 method of Minnis and Smith (1998) that was updated similar to Khaiyer et al. (2010), with some
130 modifications to more closely match those measured by the Clouds and Earth's Radiant Energy
131 System (CERES) on the Aqua and Terra satellite. The radar precipitation and satellite data are
132 3-hourly average over the analysis domain. The surface radiative fluxes and latent and sensible
133 heat fluxes are first averaged into 3-hour resolution. Then we use the Cressman's objective
134 analysis method (Cressman, 1959) to incorporate these limited number of observations with the
135 ECMWF gridded analysis and calculate the domain mean, so that the domain-mean surface
136 fluxes can better represent the entire domain. The derived large-scale vertical velocity and
137 budgets are thus representing a 3-hour average over analysis domain. The vertical resolution is
138 25 hPa.

139

140 **3. Background of Synoptic Conditions**

141 The IOP-averaged sea-level pressure and 10-meter horizontal winds from ERA-Interim
142 reanalysis (Dee et al., 2011) are plotted in Figure 2. During IOP1, the Atlantic Intertropical
143 Convergence Zone (ITCZ) was located near the Equator; while during IOP2, it was located near
144 10°N. A fourteen-day trajectory study shows that the air masses over Manaus typically come
145 from the Northern Hemisphere during IOP1 and from the Southern Hemisphere during IOP2
146 (Martin et al., 2016). The top three rows of Figure 3 show the domain-averaged zonal (u) wind,

meridional (v) wind, and relative humidity relative to liquid water, from the adjusted ECMWF analysis. Consistent with those derived from radiosonde data in Martin et al. (2016), IOP1 was dominated by northeasterly winds in the lower troposphere, with moist air throughout the troposphere; IOP2 was dominated by easterly winds in the lower troposphere, with a dry free troposphere.

The cloud frequency and domain-mean precipitation observed during IOP1 and IOP2 are shown in the remaining two rows of Figure 3. The cloud frequency was derived from the Active Remote Sensing of Clouds (ARSCL) (Kollias et al., 2007) product, which uses a combination of the 95GHz W-band ARM cloud radar (WACR), micropulse lidar (MPL), and ceilometer located at the ARM site pointing upward to determine a best-estimate cloud mask above the ARM site with 5-second temporal and 30-meter vertical resolution. The ARSCL product leverages each instrument's strengths: the WACR penetrates non-precipitating and weakly precipitating thick clouds, the MPL is sensitive to thin clouds, and the ceilometer reliably detects cloud base. The ARSCL-derived cloud mask data were then used to produce 3-hourly cloud frequencies following the method described in Xie et al. (2010b). The wet season has more cloud and precipitation events than the dry season. However, the convective systems in the dry season are typically more intense than those occurring in the wet season (Giangrande et al., 2016). Compared to 15-year climatology, the precipitation around Manaus during 2014 has a positive anomaly in IOP1 and negative anomaly in IOP2 (Burleyson et al., 2016; Martin et al., 2016). Nevertheless, the annual cycle in 2014 is still broadly representative of the climatology (Burleyson et al., 2016).

4. Seasonal Variation

In this section, we focus on the contrast between the dry and wet season large-scale vertical velocity and energy and moisture budgets. The upper row of Figure 4 shows the temporal evolution of large-scale vertical velocity in IOP1 (wet season, left) and IOP2 (dry season, right), and the IOP-mean profiles are shown as the black solid lines in the bottom row. We also define rainy (black dotted lines) and non-rain periods (gray lines) using a threshold of 0.2 mm hr^{-1}. A value of 0.2 mm hr^{-1} rather than 0 mm hr^{-1} is used because in some cases ground clutter in the SIPAM radar data may be misinterpreted as light precipitation. Changing the threshold affects the magnitude of the vertical profiles but does not change the seasonal contrast and the results of this study. Using this threshold, the percentage of the rainy period to the entire IOP is 36.9% for IOP1, but is 17.8% for IOP2, indicating that the rain frequency is an important factor impacting the seasonal mean contrast. The red and blue lines represent the mean profiles of morning (at 5 local time (LT)) precipitation systems and afternoon (at 14 LT) precipitation systems, respectively, which will be discussed in Section 5.

The non-rain vertical velocity profiles are relatively weak, with downward motion dominating in the upper troposphere during both dry and wet seasons. The rainy vertical velocity profiles show strong upward motion throughout the troposphere during both IOPs, but the level of maximum upward motion is different. The upward motion during the rainy period of IOP1 has a broad peak structure from ~700 to 300 hPa with the maximum at ~350 hPa. The 350-hPa upward motion peak is consistent with that shown in the Tropical Ocean and Global Atmosphere Coupled Ocean-Atmosphere Response Experiment (TOGA COARE) (Lin and Johnson, 1996), but lower than the peak of ~265 hPa observed in the Tropical Warm Pool-International Cloud Experiment (TWP-ICE) (Xie et al., 2010a). The upward motion during the

IOP2 rainy period also has a broad peak but the maximum is at a much lower level (~550 hPa) than in IOP1. Because the frequency of the rainy period is higher in IOP1 than in IOP2, the IOP-mean upward motion is stronger during IOP1 but weaker and limited to the lower troposphere during IOP2. As discussed in the next section, the difference in morning precipitation systems largely contributes to the seasonal contrast in the vertical velocity profiles between the wet and dry seasons.

Figures 5 and 6 show the temporal evolution and IOP-mean of apparent heating Q_1 and apparent drying Q_2 profiles, respectively. Q_1 and Q_2 were first introduced by Yanai et al. (1973) to estimate the diabatic processes:

$$Q_1 = \frac{1}{c_p}\left(\frac{\partial \bar{s}}{\partial t} + \bar{\vec{V}}\cdot\nabla\bar{s} + \bar{\omega}\frac{\partial \bar{s}}{\partial p}\right) = \frac{1}{c_p}\left(Q_{rad} + L_v(c-e) - \frac{\partial\overline{\omega' s'}}{\partial p}\right) \quad (1)$$

$$Q_2 = -\frac{L_v}{c_p}\left(\frac{\partial \bar{q}}{\partial t} + \bar{\vec{V}}\cdot\nabla\bar{q} + \bar{\omega}\frac{\partial \bar{q}}{\partial p}\right) = \frac{L_v}{c_p}\left(c - e + \frac{\partial\overline{\omega' q'}}{\partial p}\right) \quad (2)$$

where $s = c_p T + gz$ is the dry static energy and c_p is the specific heat for dry air in constant pressure; q is water vapor mixing ratio; $\vec{V}$ is horizontal wind vector; ω is vertical velocity in pressure coordinate; Q_{rad} is radiative heating; $L_v(c-e)$ is the latent heat from water condensation and evaporation (in general it also includes the latent heat and water vapor change from ice phase change); the overbar refers to a horizontal average and the prime refers to a deviation from the average. Q_1 and Q_2 are calculated from the large-scale dynamics (the first

lines of the equations) and represent the unresolved physical heat sources and moisture sinks (the second lines). Because the thermodynamic equation and water vapor conservation equation are explicitly satisfied in the variational analysis and the observed precipitation is used as the constraint, the vertical integral of $Q_1 - Q_{rad}$ and vertical integral of Q_2 are consistent with the observed precipitation rate implicitly. The vertical distributions of heating and drying profiles are important to the large-scale circulation as discussed in many other studies (e.g. Hartmann et al., 1984; Lau and Peng, 1987; Puri, 1987; Hack and Schubert, 1990).

Overall, the magnitude of Q_1 and Q_2 are consistent with Schumacher et al. (2007) for LBA at southwestern Brazilian Amazon but much smaller than Greco et al. (1994) at Manaus region. The much larger magnitude in Greco et al. (1994) is likely because it is a case study of one day. The peak height in this study is also lower than the other two studies, indicating that our cases contain more shallow cumulus and convections with low-level heating and drying.

Similar to the profiles of vertical velocity, non-rain Q_1 and Q_2 profile magnitudes in both IOPs are weak with small amounts of heating and moistening below 600 hPa indicative of non-precipitating or very weakly precipitating shallow cumulus and congestus clouds (Schumacher et al., 2008). Rainy period Q_1 and Q_2 profiles show strong heating and drying throughout the troposphere during both IOPs associated with deep convection, and both of them have double peak structures that vary between dry and wet seasons. Q_1 during IOP1 has a broad primary peak between 600 and 400 hPa, while the primary Q_1 peak during IOP2 maximizes more sharply at 550 hPa. The secondary peaks of Q_1 are at ~750 hPa in both IOPs. The peaks of Q_2 in IOP1 (at 500 and 750 hPa) are higher than those in IOP2 (at 650 and 800 hPa). The double peak features of Q_1 and Q_2 are likely due to different physical processes. For Q_1, previous studies (Johnson, 1984; Schumacher et al., 2007) interpreted the double peaks as a result from shallow

cumulus in lower level and deep convection or MCS in middle to upper level, although sometimes they superposed as one peak (Johnson, 1984). Moreover, latent cooling due to ice melting in the stratiform region may also contribute to the local minimum of Q_1 which, in some field campaigns, is only shown as an inflection (Johnson et al., 2016). Nevertheless, the local minimum or the inflection usually occurs near the melting level (~600 hPa) in many other tropical field campaigns (e.g. Schumacher et al., 2008; Xie et al., 2010a; Ahmed et al., 2016), indicating that the melting level is nearly constant in the tropics. For Q_2, the double-peak structure is the combined effect of convective (lower peak) and stratiform (higher peak) rain production (Lin and Johnson, 1996). The peak levels for stratiform and convective clouds may vary in different locations and times such as in the two IOPs in this study.

5. Diurnal Cycle

The diurnal cycles of domain mean radar-derived precipitation and surface CAPE and convective inhibition (CIN) for both IOPs are plotted in Figure 7. Precipitation in IOP1 extends from early morning to afternoon, consistent with Tanaka et al. (2014). In IOP2, most of the precipitation occurs in the afternoon. The magnitude of afternoon precipitation in IOP2 is just slightly smaller than that in IOP1, but the magnitude of morning precipitation in IOP2 is significantly lower than that in IOP1, indicating that the differences between dry and wet seasons are mainly due to the morning precipitation events. The surface CAPE has similar magnitudes in the daytime during IOP1 and IOP2, but in the early morning it rises later and slower during IOP1 than during IOP2, probably because early morning precipitation during IOP1 has released

253 atmospheric instability. The surface CIN is typically small, especially during IOP1, which is due
254 to the high surface relative humidity over the Amazon rainforest.

255 The diurnal cycles of cloud frequency, large-scale vertical velocity, Q_1, Q_2 and
256 $Q_1 - Q_2 - Q_{rad}$ for IOP1 (left) and IOP2 (right) are shown in Figure 8. Derived from Eq. (1) and
257 (2),

258 $$Q_1 - Q_2 - Q_{rad} = -\frac{1}{c_p}\frac{\partial \overline{\omega' h'}}{\partial p} \quad (3)$$

259 where $h = s + L_v q$ is the moist static energy, and Q_{rad} is estimated from using the radiative
260 transfer model in the single-column model of CAM5 (Neale et al., 2012) driven by the large-
261 scale forcing data derived from this study since it cannot be directly measured and Q_{rad} retrievals
262 from observed vertical cloud profiles (Feng et al., 2014) have not been available yet. With the
263 freezing and melting processes ignored, $Q_1 - Q_2 - Q_{rad}$ represents the vertical convergence of *h*
264 by sub-grid turbulence and cumulus.

265 Consistent with the diurnal cycles of precipitation, the observed clouds and large-scale
266 vertical velocity differ primarily in the morning between IOP1 and IOP2. In IOP1, the early
267 morning upward motion peaks at 700 hPa and extends to the upper troposphere around 200 hPa.
268 The early afternoon upward motion peaks at the upper troposphere and extends above 100 hPa.
269 Accordingly, clouds are mainly seen between 800 and 500 hPa in the early morning but
270 throughout the entire troposphere in the afternoon. In IOP2, morning convective systems are
271 generally limited to the lower levels, as shown by weak upward motion below 600 hPa and
272 downward motion above. Thus, few clouds are observed in the lower and middle troposphere
273 while some high clouds remain from the previous day's convective activities. The afternoon

convective systems are strong and deep in both IOPs, with upward motion in the upper troposphere associated with convective cloud growth and downward motion in the lower troposphere associated with convective downdrafts.

Consistent with the clouds and vertical velocity, Figure 8 also shows significant seasonal differences of Q_1 and Q_2 profiles in the morning, with heating and drying extending to the upper troposphere in IOP1 but cooling and moistening above 600-650 hPa in IOP2. In the afternoon, both IOPs show strong heating and drying in the middle and upper troposphere with weak heating and strong moistening occurring below 700 hPa. The low-level heating and moistening feature has been observed in trade wind regimes during westerly wind bursts and monsoon break periods (Nitta and Esbensen, 1974; Lin and Johnson, 1996; Johnson and Lin, 1997; Xie et al., 2010a), in which the vertical convergence of eddy fluxes and detrainment of shallow cumulus were considered as the causes. In this study it is also seen in the afternoon precipitating periods (red lines in Figure 5 and 6). To further investigate this feature, $Q_1 - Q_2 - Q_{rad}$ is shown in the last row of Figure 8. Two positive $Q_1 - Q_2 - Q_{rad}$ centers are seen during daytime between 750 to 950 hPa and between 250 to 550 hPa, respectively. It is likely that the positive $Q_1 - Q_2 - Q_{rad}$ in the lower level (below 600 hPa) is mainly due to the vertical convergence of *h* by boundary layer turbulence and shallow cumulus. The positive $Q_1 - Q_2 - Q_{rad}$ in the upper troposphere (above 600 hPa) is likely due to the vertical convergence of *h* by deep convective process. Note that $Q_1 - Q_2 - Q_{rad}$ also includes latent heat from ice freezing and melting, which may contribute to the local minimum around 600 hPa.

6. Case Studies

A set of case studies is conducted to further understand the large-scale vertical velocity and heat and moisture budgets for the three typical types of convective systems (Greco et al., 1990) that often occur in the wet season in Amazonia: locally-occurring systems (LOS), coastal-occurring systems (COS), and basin-occurring systems (BOS). Previous studies have found that LOS often occur in the afternoon characterized as scattered convections generated through solar heating at the surface, while most COS and BOS are propagating systems associated with mid-level easterlies and westerlies, respectively (e.g. Cifelli et al., 2002; Silva Dias et al., 2002a; Williams et al., 2002), and affect Manaus in the early morning. COS occurring in easterlies are often westward propagating squall-lines with intense leading lines that are more vertically developed. BOS generated in the westerlies are generally less vertically developed MCSs with a broad horizontal area and relatively homogeneous precipitation extending over a long time (Cifelli et al., 2002). Table 1 gives the number of each type of precipitation system observed during the two IOPs, identified from the radar loop (available at https://www.youtube.com/playlist?list=PLVqbwaasmlvtcu2kl_U5RaaNF0kYqW6ua) and the satellite infrared images (available at http://www-pm.larc.nasa.gov/). There are some cases in the easterlies identified as BOS because they initiated in the Amazon basin but their structures are more like COS as squall lines. More COS and BOS are seen in IOP1 than in IOP2, but the number of afternoon LOS in IOP1 is just slightly higher than that in IOP2. This again indicates that the frequency of morning propagating convective systems contributes to the variation of the diurnal cycle between the wet and dry seasons.

The three selected cases are a LOS starting from 11 LT, 13 March 2014, a COS starting from 23 LT, 20 February 2014 and a BOS starting from 17 LT, 1 March 2014. The times of these events are marked by the black lines in Figure 3. Mid-level wind was dominated by

319 westerlies on 1 March (day 60) and easterlies on 20 February (day 51). Figure 9 shows
320 representative scans of the radar reflectivity at elevation angle of 0.9° for these three cases, as
321 well as the time series of the domain mean precipitation. The LOS case has many small-scale
322 scattered convective cells that last for very short times (typically a couple of hours). Because of
323 the small horizontal coverage of the convective cells, the domain mean precipitation is less than
324 that in the other two cases. The COS case has a clear bow-shape echo indicating a squall line
325 front which moves quickly westward. The BOS case has a larger horizontal area of moderate
326 precipitation with some embedded convective cells. It moves southeastward and lasts more than
327 10 hours over the GoAmazon domain.

328 The point-observed cloud frequency and domain-averaged relative humidity, surface
329 CAPE and CIN, u- and v-winds, large-scale vertical velocity, Q_1, Q_2 and $Q_1 - Q_2 - Q_{rad}$ for the
330 three cases are shown in Figures 10-12, respectively. For the LOS case, the cloud frequency is
331 much smaller than in the other two cases, since the convective cells have small horizontal extent
332 and only occupy a small portion of the region. A shallow-to-deep transition of convective clouds
333 can be seen. The surface CAPE is large, with weak mid-level winds and moist air at the surface
334 before the convection occurred. Upward motion corresponds to the deep convection, and the
335 magnitude is smaller than in the other two cases, consistent with weaker precipitation. Starting
336 around 9 LT, Q_1 shows diabatic heating throughout the troposphere during the deep convection,
337 while Q_2 shows strong moistening between 750 and 950 hPa and weak drying above that layer.
338 The daytime positive $Q_1 - Q_2 - Q_{rad}$ between 750 and 950 hPa is mainly contributed by negative
339 Q_2 representing vertical convergence of moisture by sub-grid eddies. It can also be seen on
340 many other days during the two IOPs and are similar to the daytime profiles discussed in the
341 diurnal cycle (Section 5). Note that there is a time lag between observed cloud frequency and the

342 domain-averaged large-scale fields, which might be partially due to the fact that the cloud
343 frequency observations were taken from vertically pointing instruments at the ARM site 67.8 km
344 downwind of the center of the GoAmazon domain.

345 The COS (Figure 11) and BOS (Figure 12) cases both show a shallow-to-deep convective
346 cloud transition from the previous evening to late afternoon, with a moist lower-level atmosphere.
347 Both cases have smaller surface CAPE than the LOS case, possibly because the convective
348 systems have released the atmospheric instability in the morning. The COS case passed through
349 the GoAmazon domain around 6 LT in strong mid-level easterlies, with deep clouds and strong
350 upward motion associated with the squall line. Stratiform clouds, associated with weak upward
351 motion, remained in the upper levels until ~18 LT. Condensation from the deep convection
352 contributes to strong diabatic heating and drying throughout the troposphere, while after the
353 passage of the squall line (12-18 LT),there are some stratiform clouds remaining indicated by
354 upper-level heating/drying and lower-level cooling/moistening. The BOS case entered the
355 GoAmazon domain earlier than the COS case. In weak mid-level westerlies and descending
356 mid-to-low-level northerlies, the system moved slowly southeastward and remained in the
357 domain for a longer time. Strong upward motion related to the MCS is seen from 18 to 6 LT.
358 Large diabatic heating and drying related to the strong condensation is also seen. The remnant
359 high clouds were maintained until ~18 LT with precipitation weakening over time. The upper-
360 level heating and drying, lower-level cooling and moistening indicate that there are precipitating
361 stratiform clouds in the upper level and evaporation of precipitation underneath. The negative
362 $Q_1 - Q_2 - Q_{rad}$ in the lower level and the positive $Q_1 - Q_2 - Q_{rad}$ in the upper level are seen in both
363 the COS and BOS case, which indicates lower-level divergence of *h* and upper-level
364 convergence of *h* due to moist convective processes, consistent with Tang and Zhang (2015).

The lower-level positive $Q_1 - Q_2 - Q_{rad}$ in the afternoon is mainly contributed by the vertical convergence of moisture by sub-grid eddies, similar to that in the LOS case.

7. Summary and Discussion

This study presented the characteristics of the seasonal variation and diurnal cycle of the large-scale vertical velocity and diabatic heating (Q_1) and drying (Q_2) profiles for the two IOPs conducted during the GoAmazon2014/5 experiment. A constrained variational analysis method was used to derive the large-scale vertical velocity and Q_1 and Q_2 profiles based on surface and TOA observations and ECMWF analysis. The derived profiles correspond well with observed clouds and precipitation describing convective systems over Amazonia.

The large-scale environment over the region near Manaus has distinct seasonal variations and diurnal cycles. The wet season (IOP1) has more frequent precipitation events than the dry season (IOP2), especially in the morning. The large-scale upward motions during rainy periods have similar strength in both IOPs, however, the peak level in IOP1 is much higher than that exhibited in IOP2 (350 hPa vs. 550 hPa). Q_1 and Q_2 both have a double-peak feature during rainy period, but the physical mechanism may be different: the double peak of Q_1 may be due to the combination of shallow and deep convections and latent cooling near the melting level, while the double peak of Q_2 may be due to the different height of convective and stratiform systems. The seasonal contrast is mainly due to the higher occurrence of morning mesoscale convective systems observed during IOP1. In the morning, upward motion peaks at ~700 hPa and extends to the upper troposphere during IOP1, while it is limited to the lower levels with downward motion at the upper levels during IOP2. Afternoon convective systems have a higher vertical

motion peak than their morning counterparts, and both IOPs show similar vertical structures for the afternoon systems. The large-scale vertical velocity shows upward motion above 700 hPa and downward motion below. Accordingly, Q_1 and Q_2 also exhibit middle and upper level heating and drying related to the deep convection. Below 750 hPa, the profiles show relatively weak heating and strong moistening. This heating and moistening feature is due to the vertical convergence of heat and moisture by sub-grid eddies in the boundary layer.

Three cases from IOP1 representing different types of convective systems that often occur in the region were chosen and analyzed in this study: locally-occurring systems (LOS), coastal-occurring systems (COS) and basin-occurring systems (BOS). The LOS case was characterized by many scattered and short-lived convective cells. It had relatively weak upward motion, heating and drying in the free troposphere, and heating and moistening in the boundary layer. The COS case occurred in strong mid-level easterlies. It was characterized as a squall line with deep strong profiles of upward motion, heating and drying. The BOS case mainly happened in weak mid-level westerlies and descending mid-to-low-level northerlies. It was characterized as widespread, moderate precipitation with embedded convective cells, and lasted much longer than the other two systems. The precipitating stratiform clouds remained at upper levels for several hours evident by upper-level condensational heating and lower-level evaporative cooling. The frequency of LOS cases is similar in both IOPs while the COS and BOS events occur much more often during the wet season than the dry season. The seasonal variation of the diurnal cycle of precipitation, clouds, and environmental variables is mainly due to the COS and BOS events observed in the morning.

Previous studies have also shown that the river breeze has an important influence on the diurnal cycle near the Amazon River (e.g. dos Santos et al., 2014; Tanaka et al., 2014; Burleyson

et al., 2016) and that the impact of the local circulation can extend as far as 50 km away from the river. This local circulation and the horizontal inhomogeneity of large-scale vertical velocity, heating, and moistening could be better studied using high-resolution 3-D gridded large-scale forcing data from the three-dimensional constrained variational analysis recently developed by Tang and Zhang (2015) and Tang et al. (2016). This will be the subject of a future study.

Acknowledgment: The authors gratefully thank Luiz Machado, Jiwen Fan and many others in the GoAmazon group for valuable discussions about the synoptic and climate features in Amazonia region. This research is supported by the Biological and Environmental Research Division in the Office of Sciences of the US Department of Energy (DOE). Work at LLNL was supported by the DOE Atmospheric Radiation Measurement (ARM) program and performed under the auspices of the U. S. Department of Energy by Lawrence Livermore National Laboratory under contract No. DE-AC52-07NA27344. Work at Stony Brook was supported by the Office of Science of the U. S. Department of Energy and by the National Science Foundation. This manuscript has been authored by employees of Brookhaven Science Associates, LLC with support from the ARM program and Atmospheric Systems Research Program under Contract No. DE-AC02-98CH10886 with the U.S. Department of Energy. Dr. Zhe Feng at the Pacific Northwest National Laboratory (PNNL) is supported by the U.S. DOE, as part of the Atmospheric System Research (ASR) Program. PNNL is operated for DOE by Battelle Memorial Institute under contract DE-AC05-76RL01830. Work at ECMWF was supported by the U. S. Department of Energy via the Atmospheric Systems Research Program under Contract No. DE-SC0005259. The satellite analyses are supported by the DOE ARM and ASR Program sunder contract, DE-SC0013896. The publisher by accepting the manuscript for publication

acknowledges that the United States Government retains a non-exclusive, paid-up, irrevocable, world-wide license to publish or reproduce the published form of this manuscript, or allow others to do so, for United States Government purposes. We thank The Brazilian National Institute of Amazonian Research (INPA), the Amazonas State University (UEA) and Dr. Antonio Manzi for providing surface flux data.

References

Ahmed, F., Schumacher, C., Feng, Z., and Hagos, S.: A Retrieval of Tropical Latent Heating Using the 3D Structure of Precipitation Features, Journal of Applied Meteorology and Climatology, 55, 1965-1982, doi: doi:10.1175/JAMC-D-15-0038.1, 2016.

Atmospheric Radiation Measurement (ARM) Climate Research Facility, updated hourly. Radiative Flux Analysis (RADFLUX1LONG). 2014-02-15 to 2014-10-10, 3.21297 S 60.5981 W: ARM Mobile Facility (MAO) Manacapuru, Amazonas, Brazil; AMF1 (M1). Compiled by C. Long, K. Gaustad and L. Riihimaki. Atmospheric Radiation Measurement (ARM) Climate Research Facility Data Archive: Oak Ridge, Tennessee, USA. Data set accessed 2016-03-09 at doi: 10.5439/1179822, 1994.

Atmospheric Radiation Measurement (ARM) Climate Research Facility, updated monthly. SCM-Forcing DATA from variational analysis (VARANAL). 2014-02-18 to 2014-10-10, 3.21297 S 60.5981 W: ARM Mobile Facility (MAO) Manacapuru, Amazonas, Brazil; AMF1 (M1). Compiled by S. Tang, S. Xie and Y. Zhang. Atmospheric Radiation Measurement (ARM) Climate Research Facility Data Archive: Oak Ridge, Tennessee, USA. Data set accessed 2016-07-22 at doi: 10.5439/1273323.

Atmospheric Radiation Measurement (ARM) Climate Research Facility, updated hourly. Quality Controlled Eddy Correlation Flux Measurement (30QCECOR). 2014-02-15 to 2014-10-10, 3.21297 S 60.5981 W: ARM Mobile Facility (MAO) Manacapuru, Amazonas, Brazil; AMF1 (M1). Compiled by R. McCoy, Y. Zhang and S. Xie. Atmospheric Radiation Measurement (ARM) Climate Research Facility Data Archive: Oak Ridge, Tennessee, USA. Data set accessed 2016-03-22 at doi: 10.5439/1097546, 2003.

Burleyson, C. D., Feng, Z., Hagos, S., Fast, J., Machado, L. A. T., and Martin, S. T.: Spatial variability of the background diurnal cycle of deep convection around the GoAmazon2014/5 field campaign sites, journal of applied Meteorology and Climatology, in revision, doi, 2016.

Cifelli, R., Petersen, W. A., Carey, L. D., Rutledge, S. A., and da Silva Dias, M. A. F.: Radar observations of the kinematic, microphysical, and precipitation characteristics of two MCSs in TRMM LBA, Journal of Geophysical Research: Atmospheres, 107, LBA 44-41-LBA 44-16, doi: 10.1029/2000JD000264, 2002.

Cressman, G. P.: AN OPERATIONAL OBJECTIVE ANALYSIS SYSTEM, Monthly Weather Review, 87, 367-374, doi: doi:10.1175/1520-0493(1959)087<0367:AOOAS>2.0.CO;2, 1959.

Cutrim, E. M. C., Martin, D. W., Butzow, D. G., Silva, I. M., and Yulaeva, E.: Pilot Analysis of Hourly Rainfall in Central and Eastern Amazonia, Journal of Climate, 13, 1326-1334, doi: 10.1175/1520-0442(2000)013<1326:PAOHRI>2.0.CO;2, 2000.

Dee, D. P., Uppala, S. M., Simmons, A. J., Berrisford, P., Poli, P., Kobayashi, S., Andrae, U., Balmaseda, M. A., Balsamo, G., Bauer, P., Bechtold, P., Beljaars, A. C. M., van de Berg, L., Bidlot, J., Bormann, N., Delsol, C., Dragani, R., Fuentes, M., Geer, A. J., Haimberger, L., Healy, S. B., Hersbach, H., Hólm, E. V., Isaksen, L., Kållberg, P., Köhler, M., Matricardi, M., McNally, A. P., Monge-Sanz, B. M., Morcrette, J. J., Park, B. K., Peubey, C., de Rosnay, P., Tavolato, C., Thépaut, J. N., and Vitart, F.: The ERA-Interim reanalysis: configuration and performance of the data assimilation system, Quarterly Journal of the Royal Meteorological Society, 137, 553-597, doi: 10.1002/qj.828, 2011.

dos Santos, M. J., Silva Dias, M. A. F., and Freitas, E. D.: Influence of local circulations on wind, moisture, and precipitation close to Manaus City, Amazon Region, Brazil, Journal of Geophysical Research: Atmospheres, 119, 13,233-213,249, doi: 10.1002/2014JD021969, 2014.

Feng, Z., McFarlane, S. A., Schumacher, C., Ellis, S., Comstock, J., and Bharadwaj, N.: Constructing a Merged Cloud-Precipitation Radar Dataset for Tropical Convective Clouds during the DYNAMO/AMIE Experiment at Addu Atoll, J. Atmos. Oceanic Technol., 31, 1021-1042, doi: 10.1175/JTECH-D-13-00132.1, 2014.

Filho, A. J. P., Carbone, R. E., Tuttle, J. D., and Karam, H. A.: Convective Rainfall in Amazonia and Adjacent Tropics, Atmospheric and Climate Sciences, 5, 137-161, doi: 10.4236/acs.2015.52011, 2015.

Fu, R., Zhu, B., and Dickinson, R. E.: How Do Atmosphere and Land Surface Influence Seasonal Changes of Convection in the Tropical Amazon?, Journal of Climate, 12, 1306-1321, doi: doi:10.1175/1520-0442(1999)012<1306:HDAALS>2.0.CO;2, 1999.

Fu, R., Dickinson, R. E., Chen, M., and Wang, H.: How Do Tropical Sea Surface Temperatures Influence the Seasonal Distribution of Precipitation in the Equatorial Amazon?, Journal of Climate, 14, 4003-4026, doi: doi:10.1175/1520-0442(2001)014<4003:HDTSST>2.0.CO;2, 2001.

Giangrande, S., Toto, T., Jensen, M. P., Bartholomew, M., Feng, Z., Protat, A., Williams, C., Schumacher, C., and Machado, L.: Convective Cloud Vertical Velocity and Mass-Flux Characteristics from Radar Wind Profiler Observations During GoAmazon2014/5, Journal of Geophysical Research: Atmospheres, in review, doi, 2016.

Greco, S., Swap, R., Garstang, M., Ulanski, S., Shipham, M., Harriss, R. C., Talbot, R., Andreae, M. O., and Artaxo, P.: Rainfall and surface kinematic conditions over central Amazonia during ABLE 2B, Journal of Geophysical Research: Atmospheres, 95, 17001-17014, doi: 10.1029/JD095iD10p17001, 1990.

Greco, S., Scala, J., Halverson, J., Jr., H. L. M., Tao, W.-K., and Garstang, M.: Amazon Coastal Squall Lines. Part II: Heat and Moisture Transports, Monthly Weather Review, 122, 623-635, doi: doi:10.1175/1520-0493(1994)122<0623:ACSLPI>2.0.CO;2, 1994.

Hack, J. J., and Schubert, W. H.: Some dynamical properties of idealized thermally-forced meridional circulations in the tropics, Meteorl. Atmos. Phys., 44, 101-117, doi: 10.1007/BF01026813, 1990.

Harriss, R. C., Wofsy, S. C., Garstang, M., Browell, E. V., Molion, L. C. B., McNeal, R. J., Hoell, J. M., Bendura, R. J., Beck, S. M., Navarro, R. L., Riley, J. T., and Snell, R. L.: The Amazon Boundary Layer Experiment (ABLE 2A): dry season 1985, Journal of Geophysical Research: Atmospheres, 93, 1351-1360, doi: 10.1029/JD093iD02p01351, 1988.

Harriss, R. C., Garstang, M., Wofsy, S. C., Beck, S. M., Bendura, R. J., Coelho, J. R. B., Drewry, J. W., Hoell, J. M., Matson, P. A., McNeal, R. J., Molion, L. C. B., Navarro, R. L., Rabine, V., and Snell, R. L.: The Amazon Boundary Layer Experiment: Wet season 1987, Journal of Geophysical Research: Atmospheres, 95, 16721-16736, doi: 10.1029/JD095iD10p16721, 1990.

Hartmann, D. L., Hendon, H. H., and Houze, R. A.: Some Implications of the Mesoscale Circulations in Tropical Cloud Clusters for Large-Scale Dynamics and Climate, Journal of the Atmospheric Sciences, 41, 113-121, doi: 10.1175/1520-0469(1984)041<0113:SIOTMC>2.0.CO;2, 1984.

Janowiak, J. E., Kousky, V. E., and Joyce, R. J.: Diurnal cycle of precipitation determined from the CMORPH high spatial and temporal resolution global precipitation analyses, Journal of Geophysical Research: Atmospheres, 110, n/a-n/a, doi: 10.1029/2005JD006156, 2005.

Johnson, R. H.: Partitioning Tropical Heat and Moisture Budgets into Cumulus and Mesoscale Components: Implications for Cumulus Parameterization, Monthly Weather Review, 112, 1590-1601, doi: 10.1175/1520-0493(1984)112<1590:PTHAMB>2.0.CO;2, 1984.

Johnson, R. H., and Lin, X.: Episodic Trade Wind Regimes over the Western Pacific Warm Pool, Journal of the Atmospheric Sciences, 54, 2020-2034, doi: 10.1175/1520-0469(1997)054<2020:ETWROT>2.0.CO;2, 1997.

Johnson, R. H., Ciesielski, P. E., and Rickenbach, T. M.: A Further Look at Q1 and Q2 from TOGA COARE, Meteorological Monographs, 56, 1.1-1.12, doi: doi:10.1175/AMSMONOGRAPHS-D-15-0002.1, 2016.

Khaiyer, M., Minnis, P., Doelling, D. R., Nordeen, M. L., Palikonda, R., Rutan, D. A., and Yi, Y.: Improved TOA broadband shortwave and longwave fluxes derived from satellites over the Tropical Western Pacific, 13th Conference on Atmospheric Radiation, Am. Meteorol. Soc., Portland, OR. 27 June to 2 July, 2010.

Kollias, P., Miller, M. A., Luke, E. P., Johnson, K. L., Clothiaux, E. E., Moran, K. P., Widener, K. B., and Albrecht, B. A.: The Atmospheric Radiation Measurement Program Cloud Profiling Radars: Second-Generation Sampling Strategies, Processing, and Cloud Data Products, Journal of Atmospheric and Oceanic Technology, 24, 1199-1214, doi: 10.1175/JTECH2033.1, 2007.

Lau, K. M., and Peng, L.: Origin of Low-Frequency (Intraseasonal) Oscillations in the Tropical Atmosphere. Part I: Basic Theory, Journal of the Atmospheric Sciences, 44, 950-972, doi: 10.1175/1520-0469(1987)044<0950:OOLFOI>2.0.CO;2, 1987.

Li, W., Fu, R., and Dickinson, R. E.: Rainfall and its seasonality over the Amazon in the 21st century as assessed by the coupled models for the IPCC AR4, Journal of Geophysical Research: Atmospheres, 111, n/a-n/a, doi: 10.1029/2005JD006355, 2006.

Lin, X., and Johnson, R. H.: Heating, Moistening, and Rainfall over the Western Pacific Warm Pool during TOGA COARE, Journal of the Atmospheric Sciences, 53, 3367-3383, doi: 10.1175/1520-0469(1996)053<3367:HMAROT>2.0.CO;2, 1996.

Machado, L. A. T., Laurent, H., Dessay, N., and Miranda, I.: Seasonal and diurnal variability of convection over the Amazonia: A comparison of different vegetation types and large scale forcing, Theor Appl Climatol, 78, 61-77, doi: 10.1007/s00704-004-0044-9, 2004.

Machado, L. A. T., Silva Dias, M. A. F., Morales, C., Fisch, G., Vila, D., Albrecht, R., Goodman, S. J., Calheiros, A. J. P., Biscaro, T., Kummerow, C., Cohen, J., Fitzjarrald, D., Nascimento, E. L., Sakamoto, M. S., Cunningham, C., Chaboureau, J.-P., Petersen, W. A., Adams, D. K., Baldini, L., Angelis, C. F., Sapucci, L. F., Salio, P., Barbosa, H. M. J., Landulfo, E., Souza, R. A. F., Blakeslee, R. J., Bailey, J., Freitas, S., Lima, W. F. A., and Tokay, A.: The Chuva Project: How Does Convection Vary across Brazil?, Bulletin of the American Meteorological Society, 95, 1365-1380, doi: 10.1175/BAMS-D-13-00084.1, 2014.

Marengo, J. A., Liebmann, B., Grimm, A. M., Misra, V., Silva Dias, P. L., Cavalcanti, I. F. A., Carvalho, L. M. V., Berbery, E. H., Ambrizzi, T., Vera, C. S., Saulo, A. C., Nogues-Paegle, J., Zipser, E., Seth, A., and Alves, L. M.: Recent developments on the South American monsoon system, International Journal of Climatology, 32, 1-21, doi: 10.1002/joc.2254, 2012.

Martin, S. T., Artaxo, P., Machado, L. A. T., Manzi, A. O., Souza, R. A. F., Schumacher, C., Wang, J., Andreae, M. O., Barbosa, H. M. J., Fan, J., Fisch, G., Goldstein, A. H., Guenther, A., Jimenez, J. L., Pöschl, U., Silva Dias, M. A., Smith, J. N., and Wendisch, M.: Introduction: Observations and Modeling of the Green Ocean Amazon (GoAmazon2014/5), Atmos. Chem. Phys., 16, 4785-4797, doi: 10.5194/acp-16-4785-2016, 2016.

Minnis, P., and Harrison, E. F.: Diurnal Variability of Regional Cloud and Clear-Sky Radiative Parameters Derived from GOES Data. Part II: November 1978 Cloud Distributions, Journal of Climate and Applied Meteorology, 23, 1012-1031, doi: doi:10.1175/1520-0450(1984)023<1012:DVORCA>2.0.CO;2, 1984.

Minnis, P., and Smith, W. L.: Cloud and radiative fields derived from GOES-8 during SUCCESS and the ARM-UAV spring 1996 flight series, Geophysical Research Letters, 25, 1113-1116, doi: 10.1029/98GL00301, 1998.

577 Neale, R. B., Chen, C.-C., Gettelman, A., Lauritzen, P. H., Park, S., williamson, d., conley, a.,
578 Garcia, R., Kinnison, D., Lamarque, J., Marsh, D., Mills, M., Smith, A., Tilmes, S., Vitt, F.,
579 Morrison, H., Cameron-Smith, P., Collins, W. D., Iacono, M., Easter, R., Ghan, S. J., Liu, X.,
580 Rasch, P. J., and Taylor, M. A.: Description of the NCAR Community Atmosphere Model
581 (CAM 5.0), NCAR Technical Note NCARTN-4861STR, 274, 2012.

582 Nitta, T., and Esbensen, S.: Heat and Moisture Budget Analyses Using BOMEX Data, Monthly
583 Weather Review, 102, 17-28, doi: 10.1175/1520-0493(1974)102<0017:HAMBAU>2.0.CO;2,
584 1974.

585 Nobre, C. A., Obregón, G. O., Marengo, J. A., Fu, R., and Poveda, G.: Characteristics of
586 Amazonian Climate: Main Features, in: Amazonia and Global Change, American Geophysical
587 Union, 149-162, 2009.

588 Puri, K.: Some Experiments on the Use of Tropical Diabatic Heating Information for Initial State
589 Specification, Monthly Weather Review, 115, 1394-1406, doi: 10.1175/1520-
590 0493(1987)115<1394:SEOTUO>2.0.CO;2, 1987.

591 Schumacher, C., and Houze, R. A.: Stratiform Rain in the Tropics as Seen by the TRMM
592 Precipitation Radar*, Journal of Climate, 16, 1739-1756, doi: 10.1175/1520-
593 0442(2003)016<1739:SRITTA>2.0.CO;2, 2003.

594 Schumacher, C., Zhang, M. H., and Ciesielski, P. E.: Heating Structures of the TRMM Field
595 Campaigns, Journal of the Atmospheric Sciences, 64, 2593-2610, doi: 10.1175/JAS3938.1, 2007.

596 Schumacher, C., Ciesielski, P. E., and Zhang, M. H.: Tropical Cloud Heating Profiles: Analysis
597 from KWAJEX, Monthly Weather Review, 136, 4289-4300, doi: 10.1175/2008MWR2275.1,
598 2008.

599 Silva Dias, M. A. F., Petersen, W., Silva Dias, P. L., Cifelli, R., Betts, A. K., Longo, M., Gomes,
600 A. M., Fisch, G. F., Lima, M. A., Antonio, M. A., and Albrecht, R. I.: A case study of convective
601 organization into precipitating lines in the Southwest Amazon during the WETAMC and
602 TRMM-LBA, Journal of Geophysical Research: Atmospheres, 107, LBA 46-41-LBA 46-23, doi:
603 10.1029/2001JD000375, 2002a.

604 Silva Dias, M. A. F., Rutledge, S., Kabat, P., Silva Dias, P. L., Nobre, C., Fisch, G., Dolman, A.
605 J., Zipser, E., Garstang, M., Manzi, A. O., Fuentes, J. D., Rocha, H. R., Marengo, J., Plana-
606 Fattori, A., Sá, L. D. A., Alvalá, R. C. S., Andreae, M. O., Artaxo, P., Gielow, R., and Gatti, L.:
607 Cloud and rain processes in a biosphere-atmosphere interaction context in the Amazon Region,
608 Journal of Geophysical Research: Atmospheres, 107, LBA 39-31-LBA 39-18, doi:
609 10.1029/2001JD000335, 2002b.

610 Tanaka, L. M. d. S., Satyamurty, P., and Machado, L. A. T.: Diurnal variation of precipitation in
611 central Amazon Basin, International Journal of Climatology, 34, 3574-3584, doi:
612 10.1002/joc.3929, 2014.

613 Tang, S., and Zhang, M.: Three-dimensional constrained variational analysis: Approach and
614 application to analysis of atmospheric diabatic heating and derivative fields during an ARM SGP
615 intensive observational period, Journal of Geophysical Research: Atmospheres, 120, 7283-7299,
616 doi: 10.1002/2015JD023621, 2015.

617 Tang, S., Zhang, M., and Xie, S.: An ensemble constrained variational analysis of atmospheric
618 forcing data and its application to evaluate clouds in CAM5, Journal of Geophysical Research:
619 Atmospheres, 121, 33-48, doi: 10.1002/2015JD024167, 2016.

620 Williams, E., Rosenfeld, D., Madden, N., Gerlach, J., Gears, N., Atkinson, L., Dunnemann, N.,
621 Frostrom, G., Antonio, M., Biazon, B., Camargo, R., Franca, H., Gomes, A., Lima, M., Machado,
622 R., Manhaes, S., Nachtigall, L., Piva, H., Quintiliano, W., Machado, L., Artaxo, P., Roberts, G.,
623 Renno, N., Blakeslee, R., Bailey, J., Boccippio, D., Betts, A., Wolff, D., Roy, B., Halverson, J.,
624 Rickenbach, T., Fuentes, J., and Avelino, E.: Contrasting convective regimes over the Amazon:
625 Implications for cloud electrification, Journal of Geophysical Research: Atmospheres, 107, LBA
626 50-51-LBA 50-19, doi: 10.1029/2001JD000380, 2002.

627 Xie, S., Cederwall, R. T., and Zhang, M.: Developing long-term single-column model/cloud
628 system–resolving model forcing data using numerical weather prediction products constrained by
629 surface and top of the atmosphere observations, Journal of Geophysical Research, 109, doi:
630 10.1029/2003jd004045, 2004.

631 Xie, S., Hume, T., Jakob, C., Klein, S. A., McCoy, R. B., and Zhang, M.: Observed Large-Scale
632 Structures and Diabatic Heating and Drying Profiles during TWP-ICE, Journal of Climate, 23,
633 57-79, doi: 10.1175/2009jcli3071.1, 2010a.

634 Xie, S., McCoy, R. B., Klein, S. A., Cederwall, R. T., Wiscombe, W. J., Jensen, M. P., Johnson,
635 K. L., Clothiaux, E. E., Gaustad, K. L., Long, C. N., Mather, J. H., McFarlane, S. A., Shi, Y.,
636 Golaz, J.-C., Lin, Y., Hall, S. D., McCord, R. A., Palanisamy, G., and Turner, D. D.: CLOUDS
637 AND MORE: ARM Climate Modeling Best Estimate Data, Bulletin of the American
638 Meteorological Society, 91, 13-20, doi: 10.1175/2009BAMS2891.1, 2010b.

639 Yanai, M., Esbensen, S., and Chu, J.-H.: Determination of Bulk Properties of Tropical Cloud
640 Clusters from Large-Scale Heat and Moisture Budgets, Journal of the Atmospheric Sciences, 30,
641 611-627, doi: 10.1175/1520-0469(1973)030<0611:DOBPOT>2.0.CO;2, 1973.

642 Zhang, M., and Lin, J.: Constrained Variational Analysis of Sounding Data Based on Column-
643 Integrated Budgets of Mass, Heat, Moisture, and Momentum: Approach and Application to

644 ARM Measurements, Journal of the Atmospheric Sciences, 54, 1503-1524, doi: 10.1175/1520-
645 0469(1997)054<1503:CVAOSD>2.0.CO;2, 1997.

646 Zhang, M., Lin, J., Cederwall, R. T., Yio, J. J., and Xie, S. C.: Objective Analysis of ARM IOP
647 Data: Method and Sensitivity, Monthly Weather Review, 129, 295-311, doi: 10.1175/1520-
648 0493(2001)129<0295:OAOAID>2.0.CO;2, 2001.

649

Figure and Table Captions:

Table 1: number of convective systems identified in the morning and afternoon during IOP1 and IOP2.

Figure 1: The location of GoAmazon site in this study. The red octagon represents the analysis domain. Locations of observational sites are indicated by yellow pentagrams. Locations of cities are indicated by white dots.

Figure 2: The sea-level pressure (shaded) and 10-meter horizontal wind (vector) averaged for IOP1 (left) and IOP2 (right). The pentagram indicates the location of GoAmazon site.

Figure 3: Domain averaged time series of (from top to bottom) horizontal (u) wind, meridional (v) wind, relative humidity, cloud frequency (point observation at the ARM site) and precipitation for IOP1 (left) and IOP2 (right). The blank areas in cloud frequency indicate missing data. The three straight black lines in IOP1 show the three cases chosen in section 6.

Figure 4: The time series (top) and temporal mean profiles (bottom) of large-scale vertical velocity for IOP1 (left) and IOP2 (right).

Figure 5: The time series (top) and temporal mean profiles (bottom) of apparent heating source Q_1 for IOP1 (left) and IOP2 (right).

Figure 6: The time series (top) and temporal mean profiles (bottom) of apparent moisture sink Q_2 for IOP1 (left) and IOP2 (right).

Figure 7: The diurnal cycle of precipitation (up) and CAPE and CIN (bottom) for both IOPs.

Figure 8: The diurnal cycle of (from top to bottom) cloud frequency, large-scale vertical velocity, Q_1, Q_2 and $Q_1 - Q_2 - Q_{rad}$ for IOP1 and IOP2. The black lines are zero-lines.

Figure 9: SIPAM radar reflectivity snapshots (left) and time series of domain-mean precipitation (right) for three cases of precipitating systems. From top to bottom: LOS, COS and BOS. The black octagons indicate the GoAmazon domain, and the red arrows indicate the propagating direction of the system.

Figure 10: The time series of (a) cloud frequency, (b) relative humidity, (c) surface CAPE and CIN, (d) u wind, (e) v wind, (f) vertical velocity, (g) Q_1, (h) Q_2 and (i) $Q_1 - Q_2 - Q_{rad}$ for the LOS case. The black lines are zero-lines. The shaded and white areas in (b) indicate nightime and daytime.

Figure 11: Similar as Figure 10 but for the COS case.

Figure 12: Similar as Figure 10 but for the BOS case.

	IOP1		IOP2	
	Morning	Afternoon	Morning	Afternoon
Locally Occurring Systems (LOS)	0	19	0	16
Coastal Occurring Systems (COS)	8	2	0	1
Basin Occurring Systems (BOS)	8	1	3	2

682

683 Table 1: number of convective systems identified in the morning and afternoon during IOP1 and
684 IOP2.

685

686

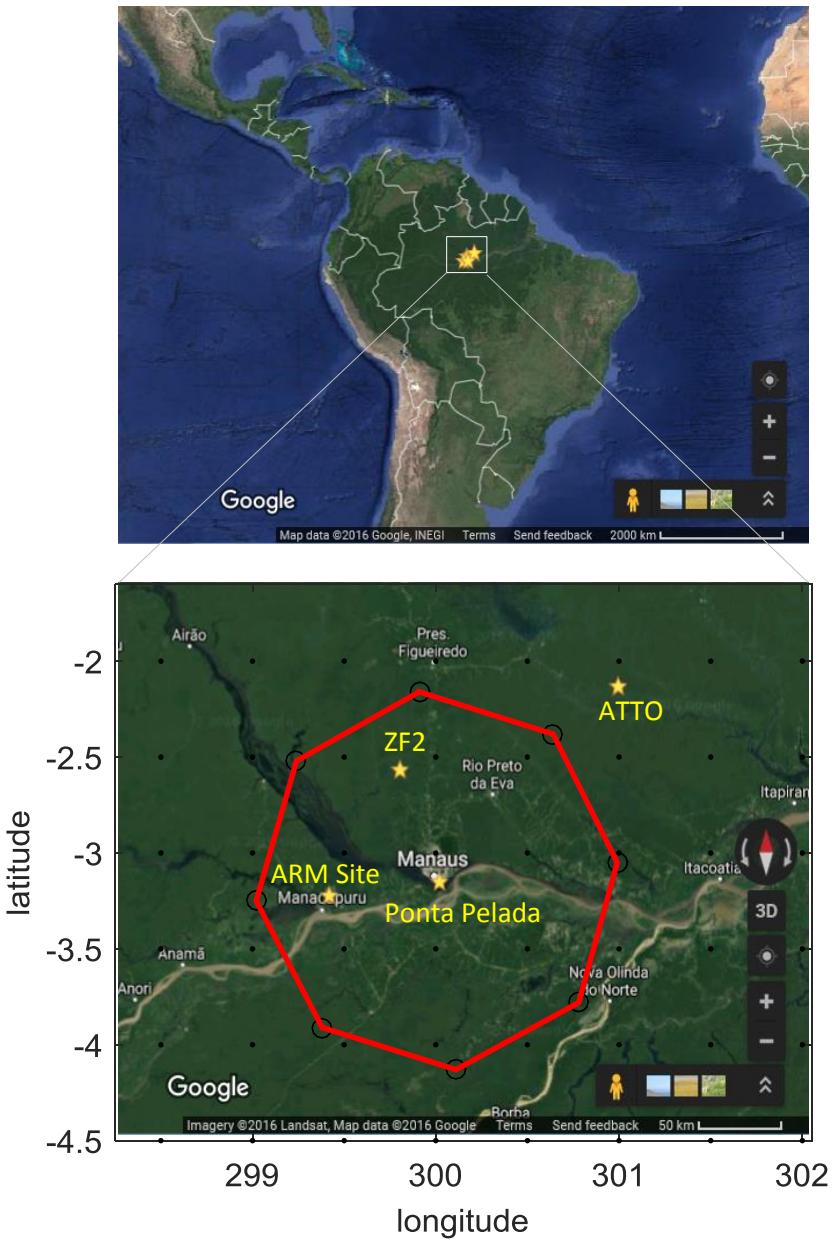

Figure 1: The location of GoAmazon site (top) and the analysis domain for this study (bottom). Locations of measurement sites are indicated by yellow pentagrams. Locations of cities are indicated by white dots.

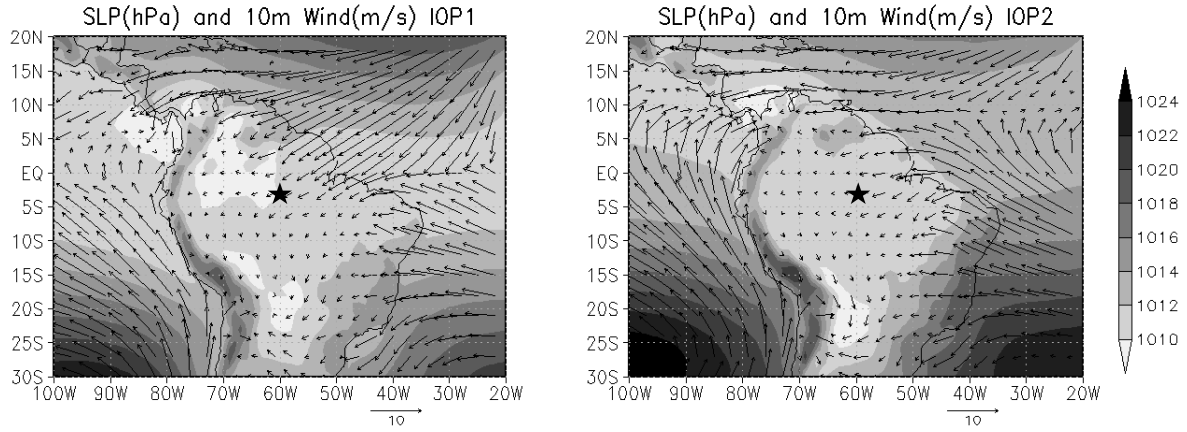

Figure 2: The sea-level pressure (shaded) and 10-meter horizontal wind (vector) averaged for IOP1 (left) and IOP2 (right). The pentagram indicates the location of GoAmazon site.

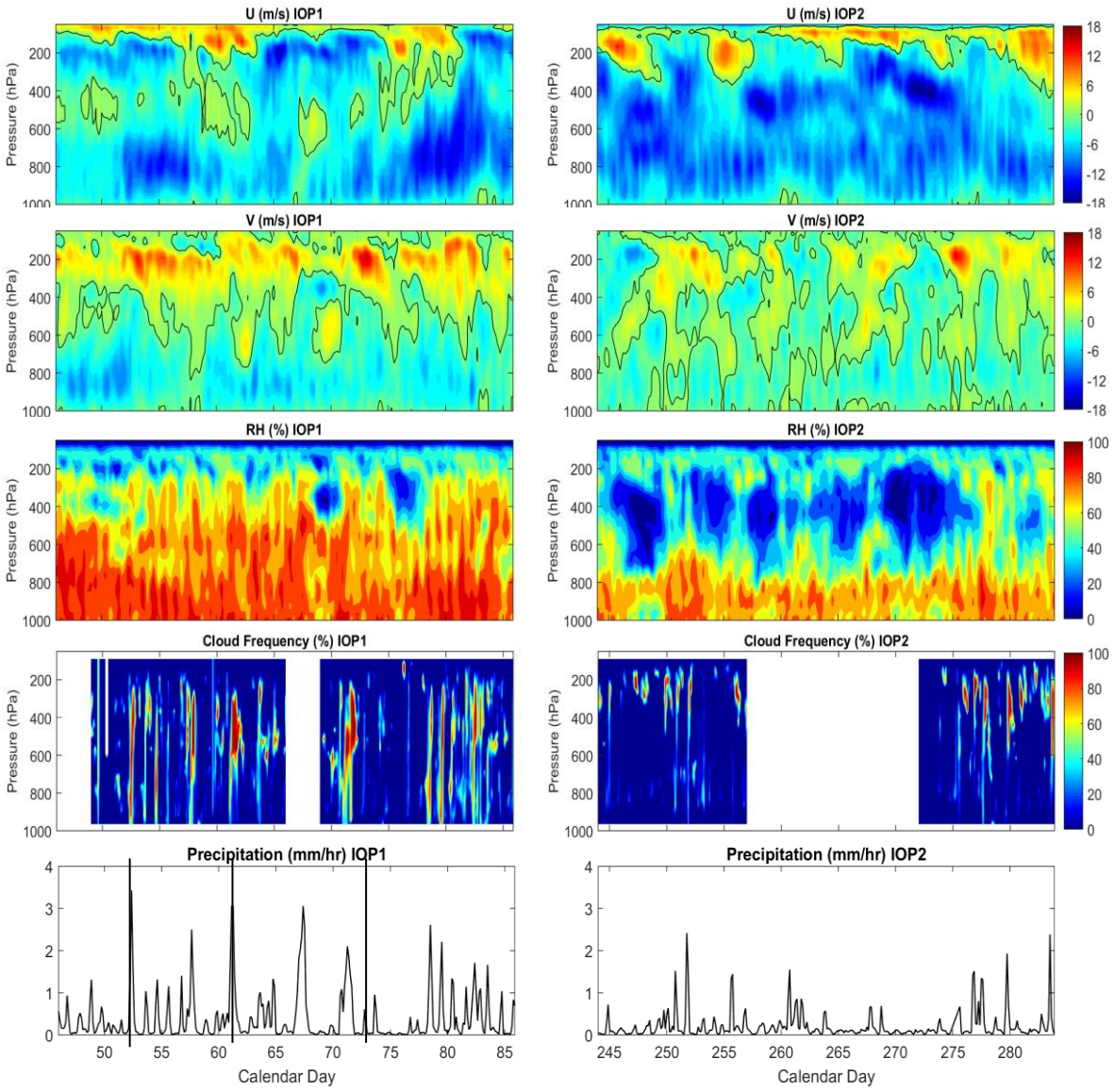

Figure 3: Domain averaged time series of (from top to bottom) horizontal (u) wind, meridional (v) wind, relative humidity, cloud frequency (point observation at the ARM site) and precipitation for IOP1 (left) and IOP2 (right). The blank areas in cloud frequency indicate missing data. The three straight black lines in IOP1 show the three cases chosen in section 6.

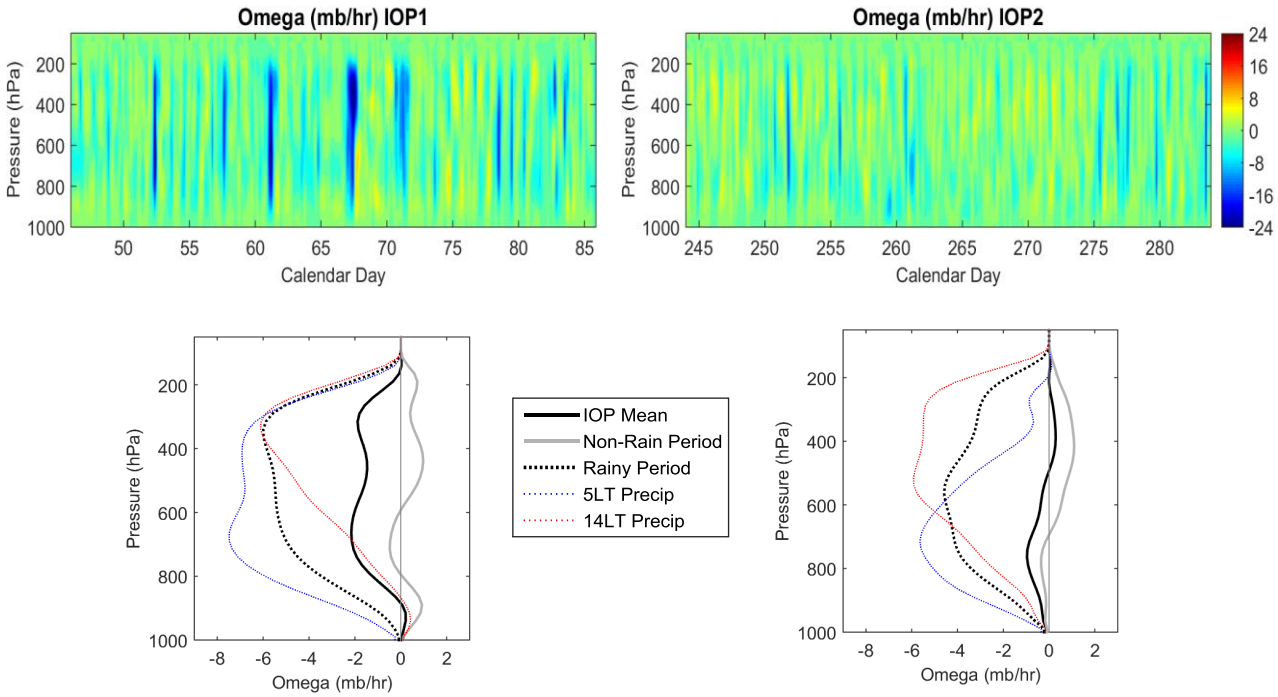

Figure 4: The time series (top) and temporal mean profiles (bottom) of large-scale vertical velocity for IOP1 (left) and IOP2 (right).

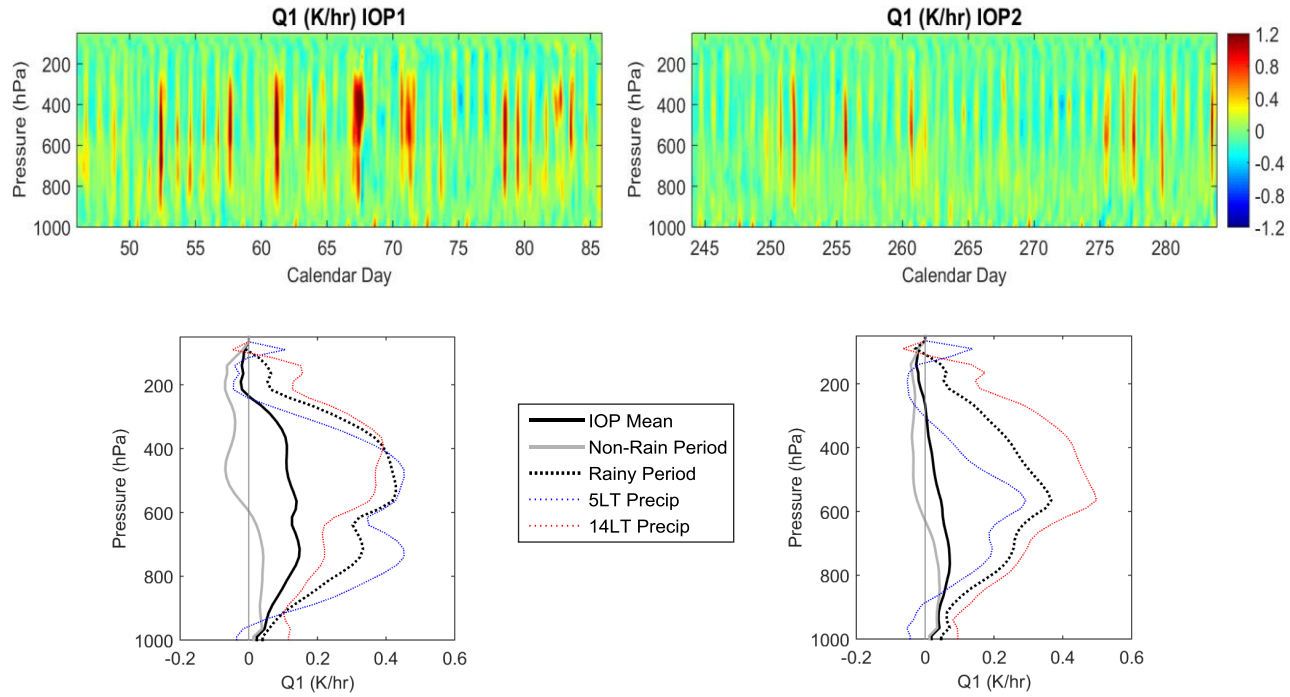

Figure 5: The time series (top) and temporal mean profiles (bottom) of apparent heating source Q_1 for IOP1 (left) and IOP2 (right).

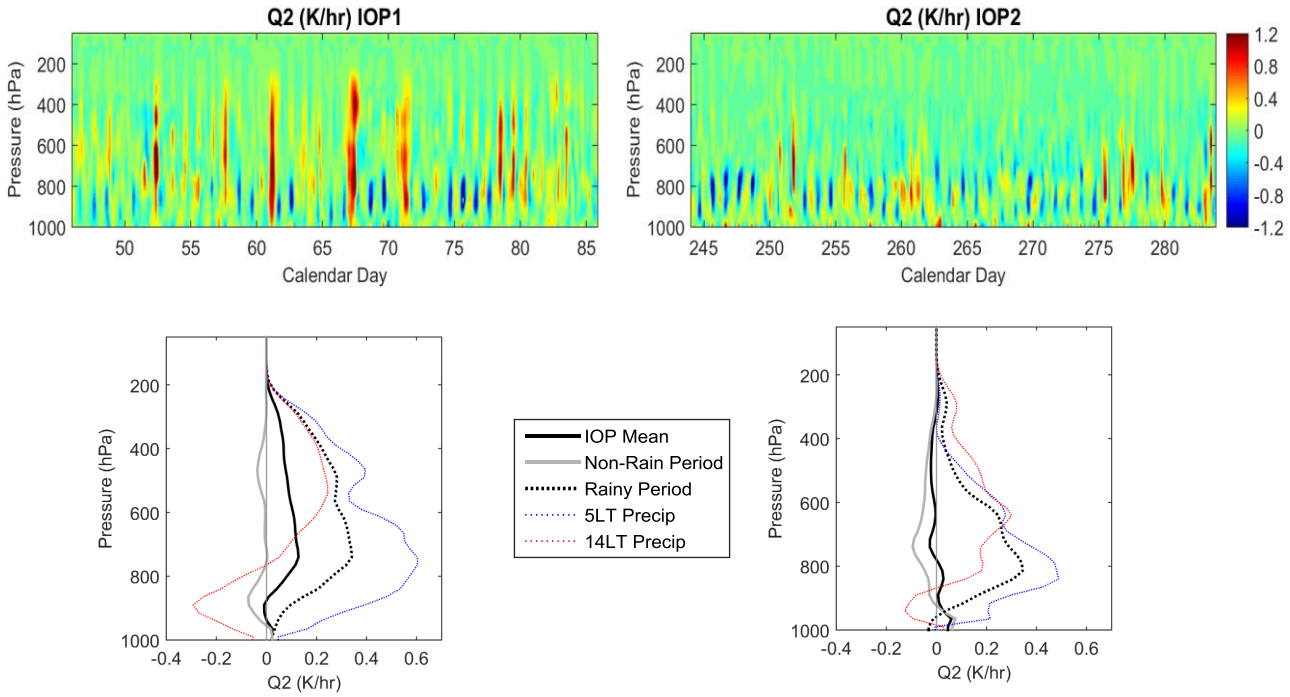

Figure 6: The time series (top) and temporal mean profiles (bottom) of apparent moisture sink Q_2 for IOP1 (left) and IOP2 (right).

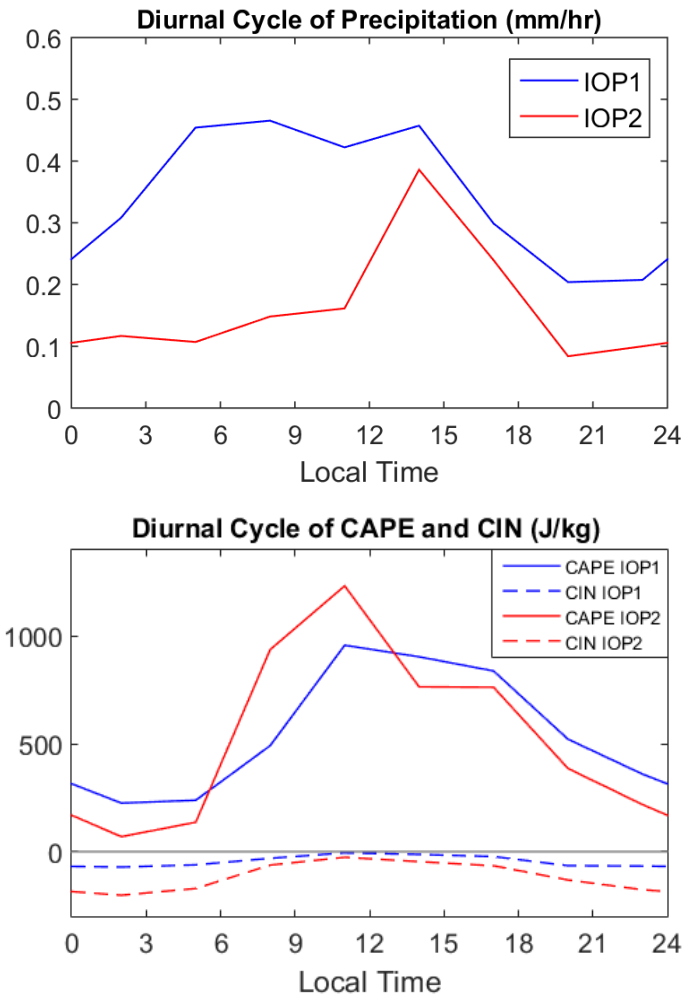

Figure 7: The diurnal cycle of precipitation (up) and CAPE and CIN (bottom) for both IOPs.

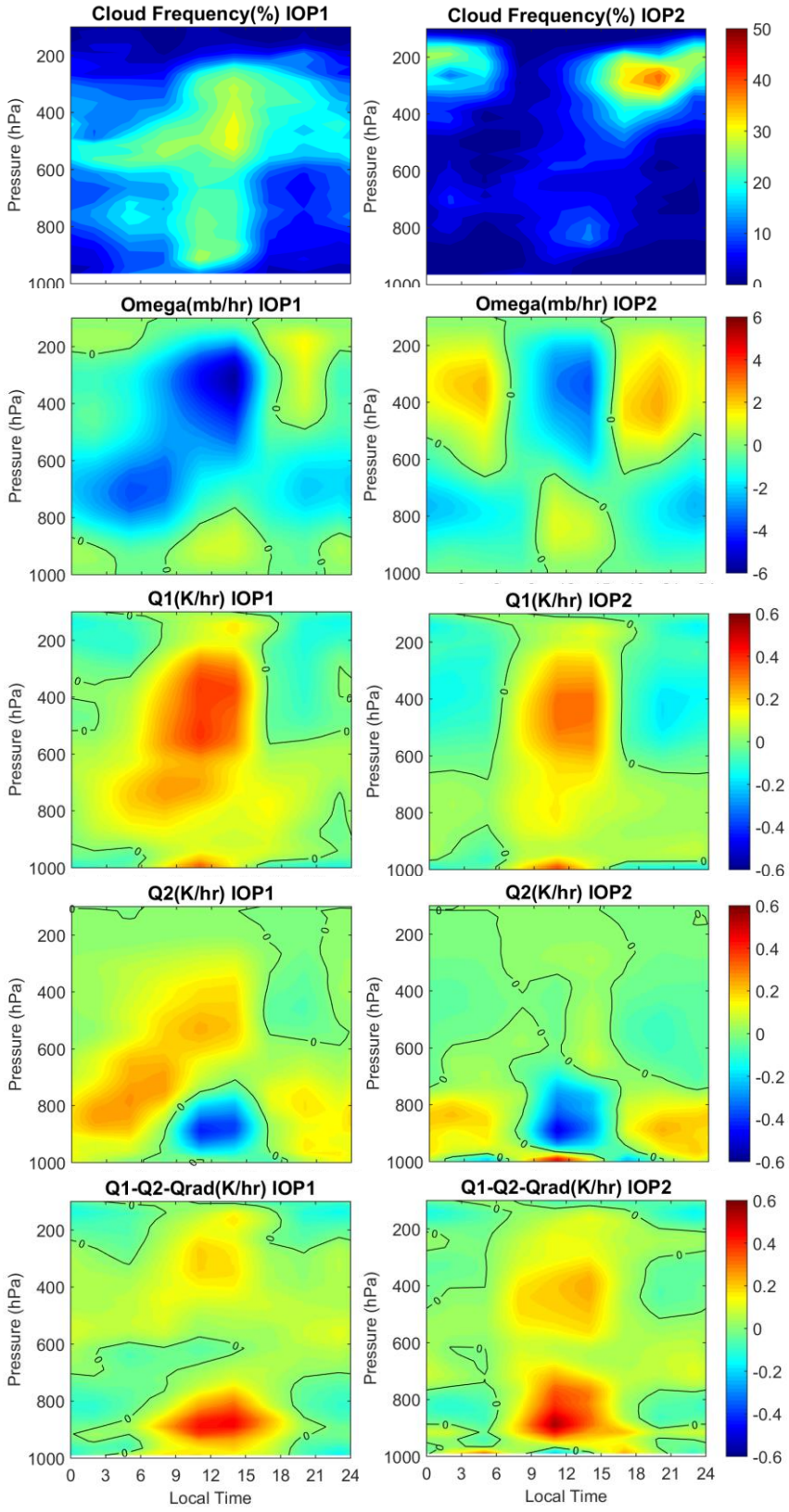

772

773 Figure 8: The diurnal cycle of (from top to bottom) cloud frequency, large-scale vertical velocity, Q_1, Q_2
774 and $Q_1 - Q_2 - Q_{rad}$ for IOP1 and IOP2. The black lines are zero-lines.

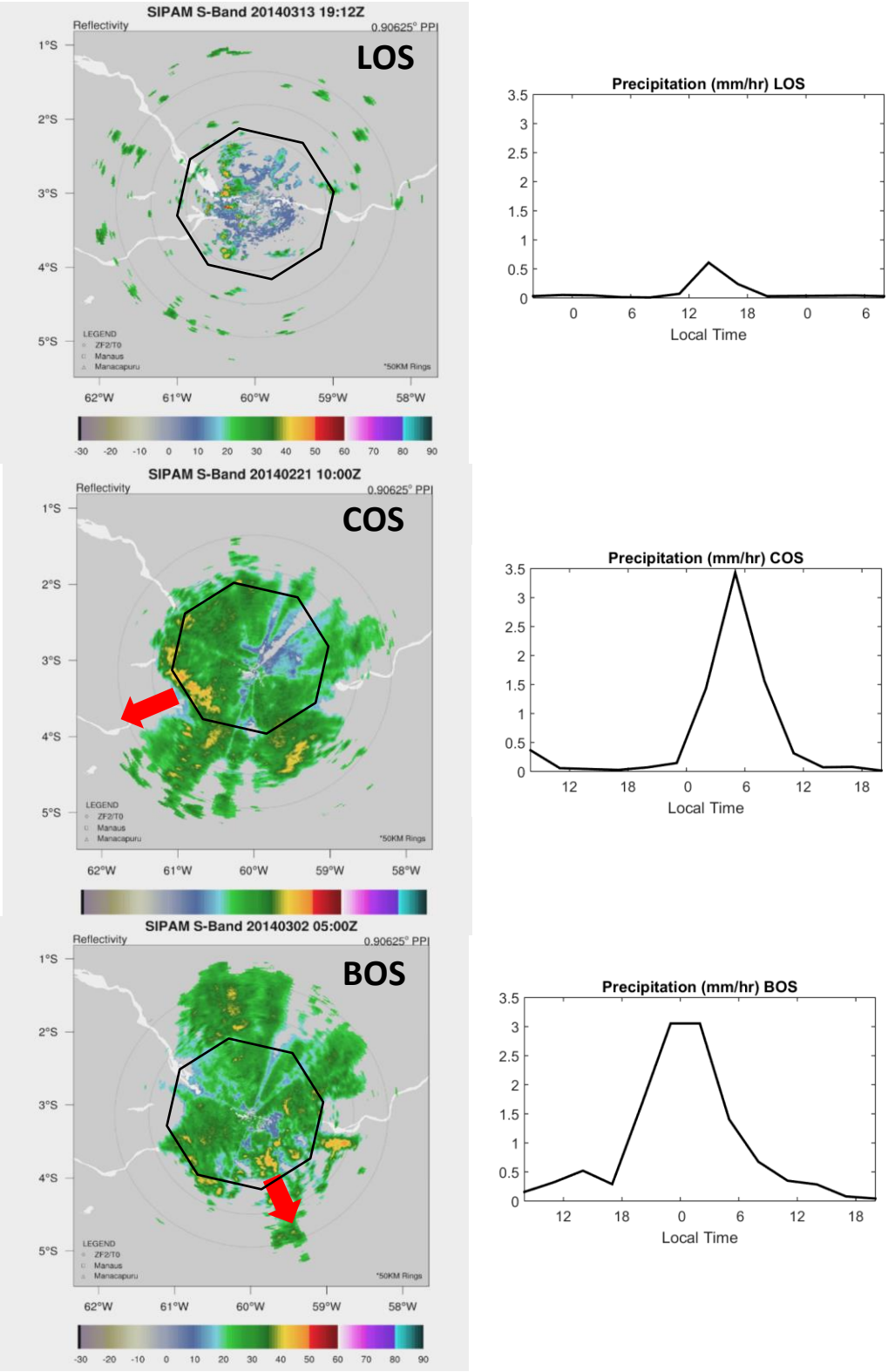

775

776 Figure 9: SIPAM radar reflectivity snapshots (left) and time series of domain-mean precipitation (right)
777 for three cases of precipitating systems. From top to bottom: LOS, COS and BOS. The black octagons
778 indicate the GoAmazon domain, and the red arrows indicate the propagating direction of the system.

779

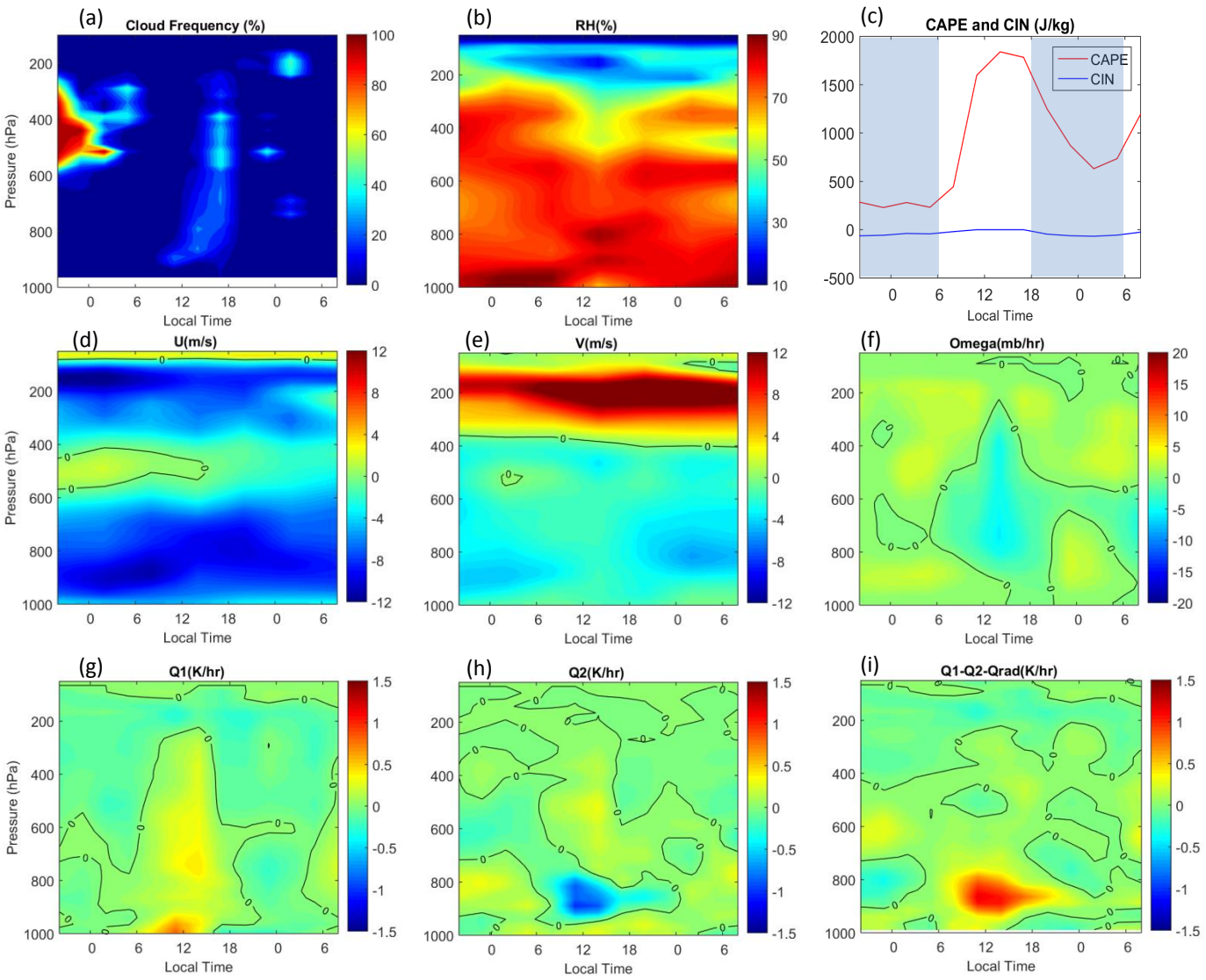

780

781 Figure 10: The time series of (a) cloud frequency, (b) relative humidity, (c) surface CAPE and CIN, (d) u
782 wind, (e) v wind, (f) vertical velocity, (g) Q_1, (h) Q_2 and (i) $Q_1 - Q_2 - Q_{rad}$ for the LOS case. The black
783 lines are zero-lines. The shaded and white areas in (c) indicate nightime and daytime.

784

785

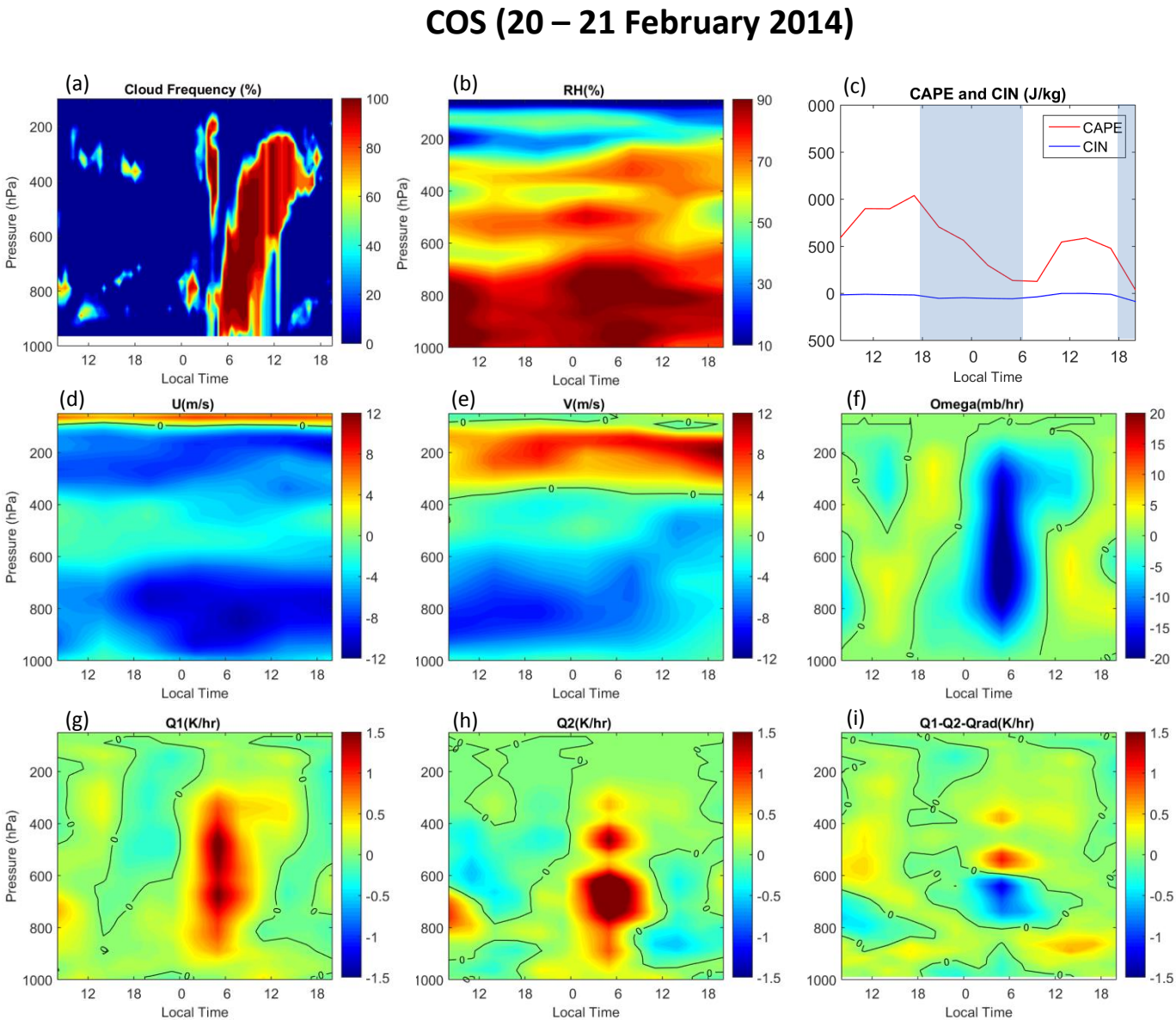

786

787 Figure 11: Similar as Figure 10 but for the COS case.

788

789

790

791

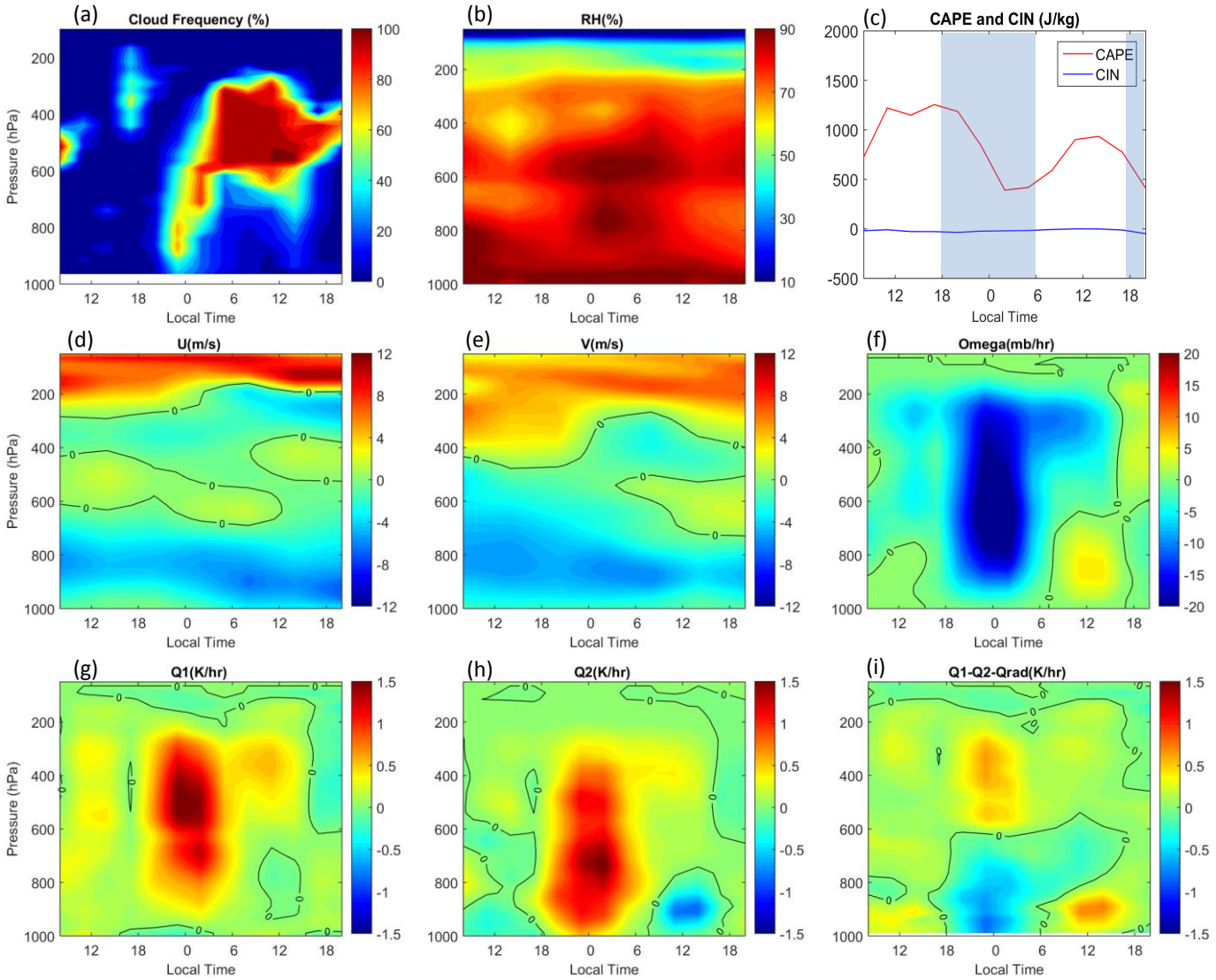

Figure 12: Similar as Figure 10 but for the BOS case.